ACCOUNTS of chemical research

Article

pubs.acs.org/accounts

Modeling Materials and Processes in Hybrid/Organic Photovoltaics: From Dye-Sensitized to Perovskite Solar Cells

Filippo De Angelis*

Computational Laboratory for Hybrid/Organic Photovoltaics (CLHYO), CNR-ISTM, Via Elce di Sotto 8, 06123 Perugia, Italy

Supporting Information

CONSPECTUS: Over the last 2 decades, researchers have invested enormous research effort into hybrid/organic photovoltaics, leading to the recent launch of the first commercial products that use this technology. Dye-sensitized solar cells (DSCs) have shown clear advantages over competing technologies. The top certified efficiency of DSCs exceeds 11%, and the laboratory-cell efficiency is greater than 13%. In 2012, the first reports of high efficiency solid-state DSCs based on organohalide lead perovskites completely revolutionized the field. These materials are used as light absorbers in DSCs and as light-harvesting materials and electron conductors in meso-superstructured and flat heterojunction solar cells and show certified efficiencies that exceed 17%.

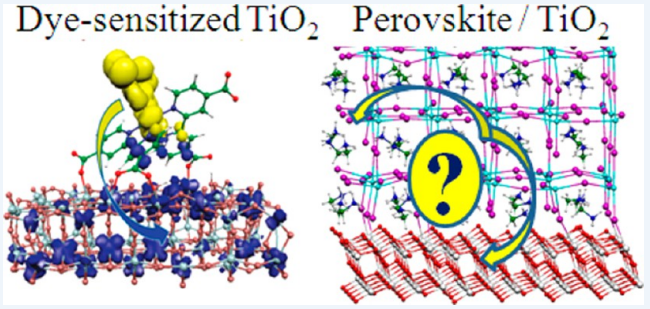

To effectively compete with conventional photovoltaics, emerging technologies such as DSCs need to achieve higher efficiency and stability, while maintaining low production costs. Many of the advances in the DSC field have relied on the computational design and screening of new materials, with researchers examining material characteristics that can improve device performance or stability. Suitable modeling strategies allow researchers to observe the otherwise inaccessible but crucial heterointerfaces that control the operation of DSCs, offering the opportunity to develop new and more efficient materials and optimize processes. In this Account, we present a unified view of recent computational modeling research examining DSCs, illustrating how the principles and simulation tools used for these systems can also be adapted to study the emerging field of perovskite solar cells. Researchers have widely applied first-principles modeling to the DSC field and, more recently, to perovskite-based solar cells. DFT/TDDFT methods provide the basic framework to describe most of the desired materials and interfacial properties, and Car−Parrinello molecular dynamics allow researchers the further ability to sample local minima and dynamical fluctuations at finite temperatures. However, conventional DFT/TDDFT has some limitations, which can be overcome in part by tailored solutions or using many body perturbation theory within the GW approach, which is however more computationally intensive. Relativistic effects, such as spin−orbit coupling, are also included in simulations since they are fundamental for addressing systems that contain heavy atoms. We illustrate the performance of the proposed simulation toolbox along with the fundamental modeling strategies using selected examples of relevant isolated device constituents, including dye and perovskite absorbers, metal-oxide surfaces and nanoparticles, and hole transporters. We critically assess the accuracy of various computational approaches against the related experimental data. We analyze the representative interfaces that control the operational mechanism of the devices, including dye-sensitized TiO_2/hole transporter and organohalide lead perovskite/TiO_2, and the results reveal fundamental aspects of the device's operational mechanism. Although the modeling of DSCs is relatively mature, the recent "perovskite storm" has presented new problems and new modeling challenges, such as understanding exciton formation and dissociation at interfaces and carrier recombination in these materials.

1. INTRODUCTION

Solar technologies, in particular photovoltaics, are foreseen as a major source of renewable energy. Hybrid/organic photovoltaics has witnessed a huge research effort in the last 2 decades, recently leading to the first commercial products. Dye-sensitized solar cells (DSCs)[1] have maintained a clear lead in efficiency and stability over competitive technologies, with top certified efficiency exceeding 11% and laboratory-cell efficiency above 13%.[2] Crucial to functioning of the DSCs is the photoinduced charge separation occurring at the heterointerface(s) between a sensitized metal-oxide electrode, typically TiO_2, and a hole transporter (HT), Scheme 1a. Grafted on the oxide surface is a monolayer of sensitizing dye, which absorbs the solar radiation and injects photoexcited electrons into the semiconductor conduction band (CB). The oxidized dye is reduced by the hole transporter, which is in turn reduced at the counter-electrode, closing the circuit. The highest DSC efficiency has been obtained with a liquid hole transporter, I^-/I_3^- or Co(II)/Co(III) redox couples in organic solvents.

Special Issue: DFT Elucidation of Materials Properties

Received: February 28, 2014
Published: May 23, 2014

   dx.doi.org/10.1021/ar500089n | Acc. Chem. Res. 2014, 47, 3349−3360

Scheme 1. Energy Levels and Schematic Operational Mechanism of (a) DSCs, (b) perovskite based DSCs (TiO_2) or MSSCs (Al_2O_3), and (c) Perovskite Flat Heterojunction[a]

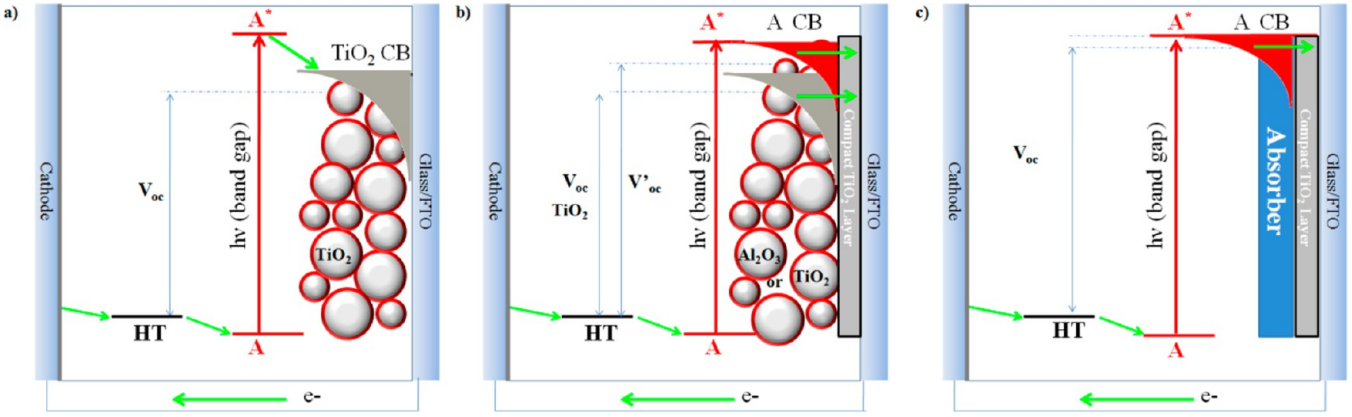

[a]The TiO_2 DOS is represented by gray and the perovskite DOS by red areas.

The field has been completely revolutionized in 2012 by the first reports of high efficiency solid-state DSCs based on organohalide perovskites (e.g., methylammonium lead iodide, $MAPbI_3$) as light absorbers,[3] Scheme 1b, which led to 15% efficiency.[4] Lee et al.[5] further demonstrated that a similar perovskite can serve both as light harvesting material and as electron conductor in meso-superstructured solar cells (MSSCs), currently exceeding 15% efficiency. These devices, in which TiO_2 was replaced by an insulating Al_2O_3 scaffold, represent a new generation of photovoltaic devices. The field further evolved toward a planar heterojunction incorporating a vapor-deposited perovskite, Scheme 1c, which exceeded 15% efficiency.[6]

First-principles modeling has been widely applied to the DSC field[7−10] and more recently to perovskite-based solar cells.[11−13] On the one hand, one wishes to design and screen new materials, with tailored and engineered characteristics for improved device performance and stability. On the other hand, modeling may offer a hitherto inaccessible view of the heterointerfaces ruling the device operational mechanism.

To effectively compete with existing photovoltaics, emerging technologies need to achieve high efficiency and stability, maintaining low production costs. The solar cell efficiency (η) is defined as

$$\eta = \frac{J_{sc} V_{oc} \mathrm{FF}}{P_I} \tag{1}$$

where J_{sc} is the photocurrent density at short circuit, FF is the cell fill factor, P_I is the intensity of the incident light, and V_{oc} is the open circuit voltage of the cell, whose definition in terms of energy levels varies with the type of device, Scheme 1.

J_{sc} is the integral over the solar spectrum of the monochromatic incident photon-to-current conversion efficiency (IPCE) under short circuit conditions, and as such it depends directly on the absorber. The DSCs V_{oc} represents the difference between the quasi-Fermi level of the metal oxide under illumination and the hole transporter redox potential, Scheme 1a, the latter being nearly constant. In DSCs, V_{oc} depends only indirectly on the absorber, while the absorber CB energy fixes the device V_{oc} in MSSCs and in flat heterojunctions, Scheme 1b,c. The FF is an adimensional parameter that reflects the shape of the $J-V$ curve.

A computational approach to hybrid/organic photovoltaics can be cast into a stepwise problem, whereby one needs to accurately simulate the individual components, to move to the relevant heterointerfaces. The fundamental information required on individual materials is (i) the absorber structures, energy levels, and optical absorption spectra, (ii) a model for the metal-oxide surface, along with its CB energy and density of states, and (iii) the hole-transporter oxidation potential. This information constitutes the basis for the design and screening of new materials, and thus a fast and effective computational tool is required.

For the interacting absorber/metal oxide/hole transporter, one needs to calculate (i) the interface structure and (ii) the nature/localization of excited states and the energy level alignment. An alternative strategy, not discussed here, is the explicit simulation of photoinduced electron transfers relevant to DSCs by quantum or nonadiabatic dynamics.[8,15]

Density functional theory (DFT) and time-dependent DFT (TDDFT) provide the framework to describe most of the desired materials and interfacial properties. DFT-based Car−Parrinello molecular dynamics[14] further allows us to sample the investigated systems at finite temperature. Conventional DFT/TDDFT have however some limitations in the description of dispersion interactions, of semiconductor band gaps, and of charge-transfer excited states; thus specifically tailored DFT approaches can be adopted. Many body perturbation theory, within the GW approach, constitutes a solid framework to improve upon DFT. GW is however (much) more computationally demanding than DFT, limiting its routine application. A general issue with all computational tools is the inclusion of relativistic effects. These are usually approximated by scalar-relativistic (SR) and, to higher order, by spin−orbit coupling (SOC) contributions, and they cannot be neglected in heavy-element-containing systems.

In this Account, I offer a unified view of recent activity in the computational modeling of DSCs, illustrating how the same principles and simulation tools, properly adapted, can be employed in the emerging field of perovskite solar cells. The challenges and unsolved issues are highlighted.

dx.doi.org/10.1021/ar500089n | Acc. Chem. Res. 2014, 47, 3349−3360

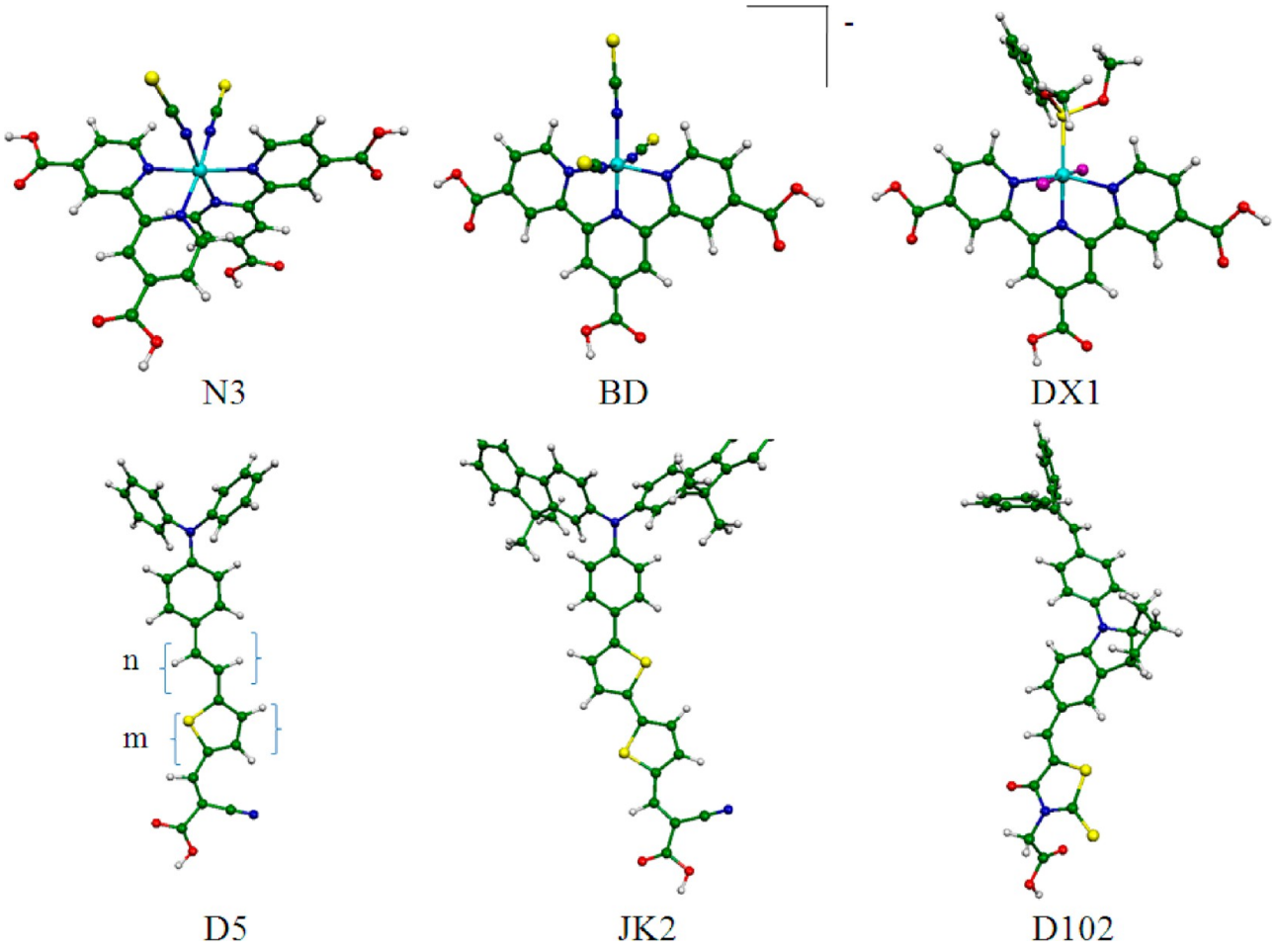

Figure 1. Calculated structures of selected ruthenium (top) and organic dyes (bottom).

2. MODELING INDIVIDUAL DEVICE COMPONENTS

2.1. Dye Sensitizers

Ru(II)−polypyridyl complexes, such as the N3, N719,[16] and black dye, Figure 1, had a central role in advancing DSC technology. A novel black-dye-like *trans*-dichloro-Ru(II) dye was recently reported,[17] DX1 in Figure 1, which showed enhanced spectral response in the 700−900 nm region allowing demonstration of a record J_{sc}. Fully organic push−pull sensitizers, Figure 1, have been developed because of their increased molar extinction coefficient, spectral tunability, and reduced environmental impact. Functionalized donor−acceptor Zn(II)-porphyrins have more recently emerged as a new class of sensitizers with high performance, due to their extended absorption spectrum.[2]

Standard DFT/TDDFT including solvation effects proved to be extremely successful in reproducing the electronic and optical properties of ruthenium dyes, Figure 2a,b;[18,19] the ground and excited state oxidation potentials of the N3/N719 dyes were calculated within <0.1 eV of the experimental values.[20] This has opened the way to the routine calculation of existing and new dyes, allowing the fast screening of new molecules in terms of their energy levels and absorption spectra in just few hours of computer time.[20] The easiness in computationally describe ruthenium dyes is their d^6 closed shell ground state and the relatively low charge-transfer degree of their excited states.

Most notably, the investigated ruthenium dyes, for example, N3 or black dye, were nicely calculated without inclusion of relativistic effects. Significantly, however, the enhanced DX1 spectral response was attributed to SOC-promoted spin-forbidden transitions.[17] The electronic and optical properties of the panchromatic black dye and DX1 dyes were thus investigated by SR- and SOC-TDDFT,[21,22] employing B3LYP and a continuum solvation model, see Figure 2a,b for a comparison between simulated and experimental spectra.

The room-temperature spectra of black dye and DX1 are nicely reproduced by both SR- and SOC-TDDFT, the latter introducing only a slight spectral broadening in the lower energy range. Also, the energy of the lowest dye excited state, relevant to set the energetics of electron injection onto TiO_2, is marginally affected by SOC. To further quantify the impact of SOC, we compared our calculations with the low-temperature DX1 absorption spectrum. Figure 2c highlights two excitations originated by mixing of the lowest singlet excited state with low-lying triplet excitations. The calculated molar extinction coefficient of DX1, 2988 M^{-1} cm^{-1} at 1.58 eV, is in excellent agreement with the ∼3000 M^{-1} cm^{-1} experimental value. We thus estimated the impact of SOC on the IPCE and J_{sc} generation due to the lowest absorption band (from 1.3 to 1.9 eV), Figure 2d. Assuming a 0.5 M dye concentration, a 10 μm film thickness, and a unitary injection and collection efficiency, we can calculate IPCE(λ).[21] The results highlight how SOC contributes an overall J_{sc} gain of 2.3 mA/cm^2 in the

dx.doi.org/10.1021/ar500089n | *Acc. Chem. Res.* 2014, 47, 3349−3360

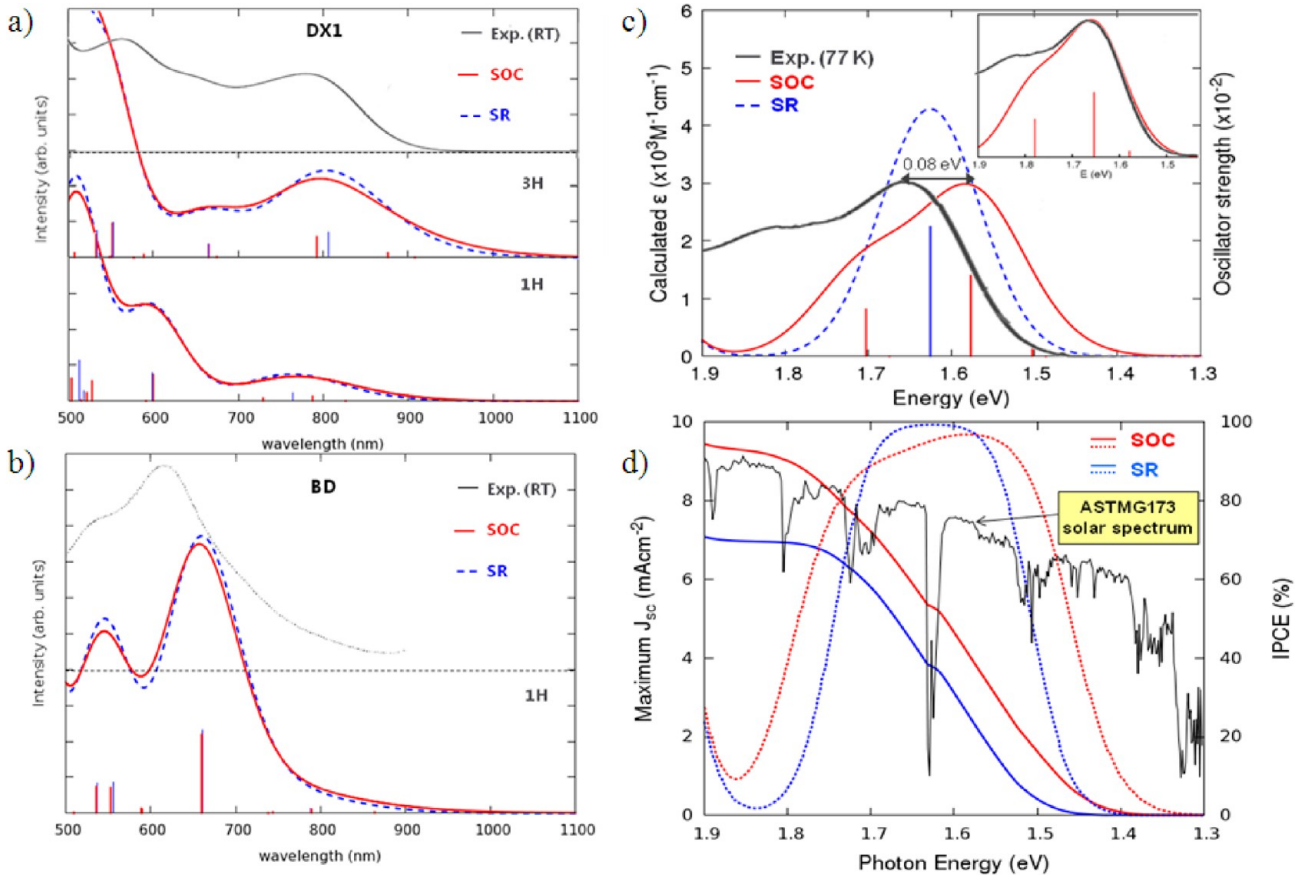

Figure 2. (a,b) Experimental UV−vis spectrum of DX1 and black dye (BD, black solid lines) at room temperature and calculated absorption of fully protonated (3H) and monoprotonated (1H) dyes by SR- (blue) and SOC-TDDFT (red), using a Gaussian broadening with σ = 0.12 eV. (c) Experimental spectrum of DX1 (black) at 77 K compared with the SR- and SOC-simulated spectra with σ = 0.08 eV. Inset: same but shifted by 0.08 eV. (d) Maximum J_{sc} (mA/cm^2, dotted lines) and IPCE curve (%, full lines) computed by SR (blue) and SOC (red) levels against the ASTMG173 solar spectrum (black). In panels a−c, blue (red) vertical lines correspond to SR (SOC)-calculated oscillator strengths.

low energy region, amounting to ca. 10% of the total J_{sc} extracted from DX1-based DSCs.

The calculation of excitation energies of push−pull organic dyes turned out to be a more complicated issue.[23−25] TDDFT yields large underestimations for excited states with a significant long-range charge-transfer character. The use of hybrid functionals incorporating an increased amount of Hartree−Fock exchange, for example, MPW1K, partially corrects this issue, but the correction remains system-dependent. Long-range corrected functionals and the Coulomb-attenuating B3LYP (CAM-B3LYP) method partly remedy this problem. Here we discuss the performance of TDDFT for two representative dyes having different electron donor and acceptor groups, the conjugated JK-2 and the nonconjugated D102 dye, Figure 1.

In Table 1, we report the calculated lowest excitation energies for the considered dyes along with experimental absorption maxima. JK2 data calculated by MPW1K and CAM-B3LYP are in good agreement with experimental data, while B3LYP substantially underestimates the lowest excitation energy. For D102, we find a similar trend although in this case both MPW1K and CAM-B3LYP seem to overshoot the experimental data, while B3LYP underestimates the absorption energy. Clearly the JK2 and D102 dyes have quite a different response to the choice of the DFT method. This system-dependent variability imposes a careful calibration of the computational protocol. Furthermore, when calculating conjugated organic dyes adsorbed onto TiO_2, CAM-B3LYP (and MPW1K) convey the correct excitation energy but substantially overshoot the TiO_2 CB energy and band gap, leading to an unphysical excited state alignment.[25] B3LYP, on the other hand, underestimates the (adsorbed) dye excitation energy but nicely reproduces the TiO_2 CB energy and band gap.[25] At present, we have found no solution to this issue within TDDFT.

Table 1. Calculated (B3LYP/6-311G*) and Experimental Lowest Excitation Energies (eV) for the Protonated JK2 and D102 Dyes in Ethanol

dye	B3LYP	MPW1K	CAM-B3LYP	expt
JK2	1.82	2.45	2.62	2.84
D102	2.29	2.78	2.86	2.53

The calculation of the oxidation potential of organic dyes also turned out to be a challenging task.[24] For a set of four triphenylamine-based dyes, related to D5 in Figure 1, with increasing degree of conjugation, the accuracy of all the employed DFT methods deteriorates, against the experimental trend, as the dye conjugation increases, Figure 3. Increasing the fraction of Hartree−Fock exchange does not improve the calculated trend. Encouragingly, GW calculations suggested an improved trend compared with DFT. The vertical ionization potential for the (n = 0/m = 0) and (n = 1/m = 1) systems

dx.doi.org/10.1021/ar500089n | Acc. Chem. Res. 2014, 47, 3349−3360

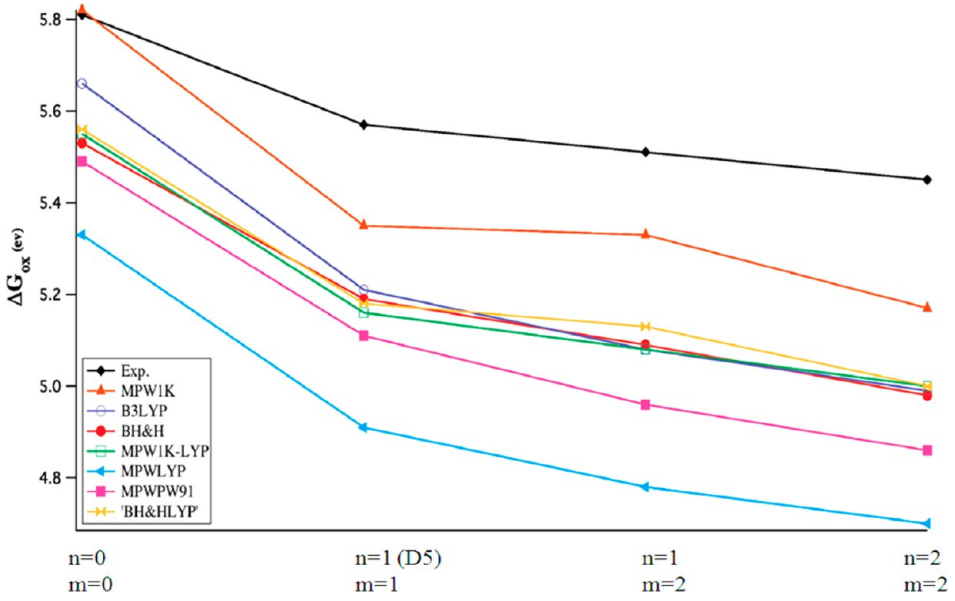

Figure 3. Experimental and calculated oxidation potentials in acetonitrile solution by various DFT methods for the dye series derived from D5, with varying number of double C═C bonds (n) and thiophene units (m).

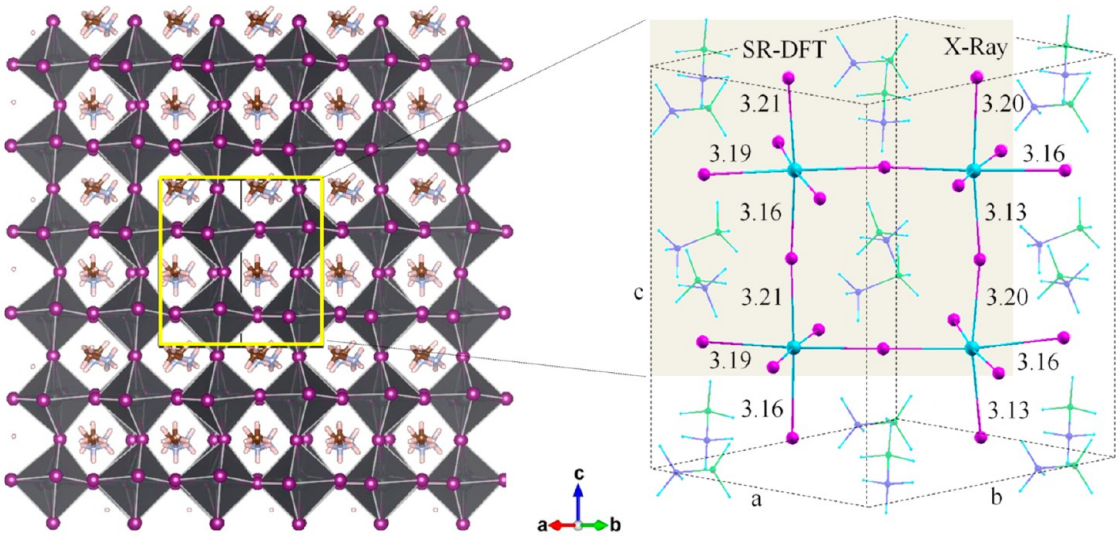

Figure 4. Calculated structure of $MAPbI_3$ along with main distances (Å). The unit cell (highlighted in yellow in the left panel) corresponds to the shaded area on the right panel.

were calculated at 6.87/6.48 eV, compared with experimental values of 6.75/6.50 eV.[26]

2.2. Organohalide Perovskites

The $MAPbI_3$ and $MAPb(I_{1-x}Cl_x)_3$ perovskites (MA = $CH_3NH_3^+$) have dominated the field of perovskite solar cells.[4,6] The high photovoltaic efficiency is partly related to the optimal $MAPbI_3/MAPbI_{3-x}Cl_x$ band gap (1.5−1.6 eV), which directly influences J_{sc} and contributes to V_{oc}, Scheme 1b,c. The similar $MASnI_3$ perovskite has been less explored for photovoltaic applications, despite showing a reduced band gap (∼1.2 eV). Replacement of Pb by the more environmentally friendly Sn is obviously highly attractive for a large-scale technology uptake.

Standard DFT (PBE) provides reliable structures and stabilities of organohalide perovskites.[11] Contrary to expectations,[27] the calculated band gaps of $MAPbI_3$ by SR-DFT were in surprisingly good agreement, within ±0.1 eV, with experimental values. For the supposedly similar $ASnX_3$ perovskites, SR-DFT provides a ∼1 eV band gap underestimate. Such an unbalanced description of Sn- and Pb-based perovskites hampers any predictive or comparative materials design and screening. The calculated band gap difference between $ASnX_3$ and $APbX_3$ perovskites might be due to relativistic effects.[11] A strong SOC effect and associated band-gap underestimate was indeed calculated for $MAPbI_3$ by SOC-DFT.[12] To solve this issue, a computationally affordable GW approach incorporating SOC[28] was very recently devised by Umari et al. and applied to $MAPbI_3$ and $MASnI_3$.[13] Structural optimization of $MAPbI_3$ and $MASnI_3$, performed on a 48 atom unit cell, Figure 4, led to calculated bond lengths and lattice parameters in good agreement (within 1−2%) with experimental data, Figure 4. The band gaps calculated at various levels of theory are graphically represented in Figure 5.

dx.doi.org/10.1021/ar500089n | Acc. Chem. Res. 2014, 47, 3349−3360

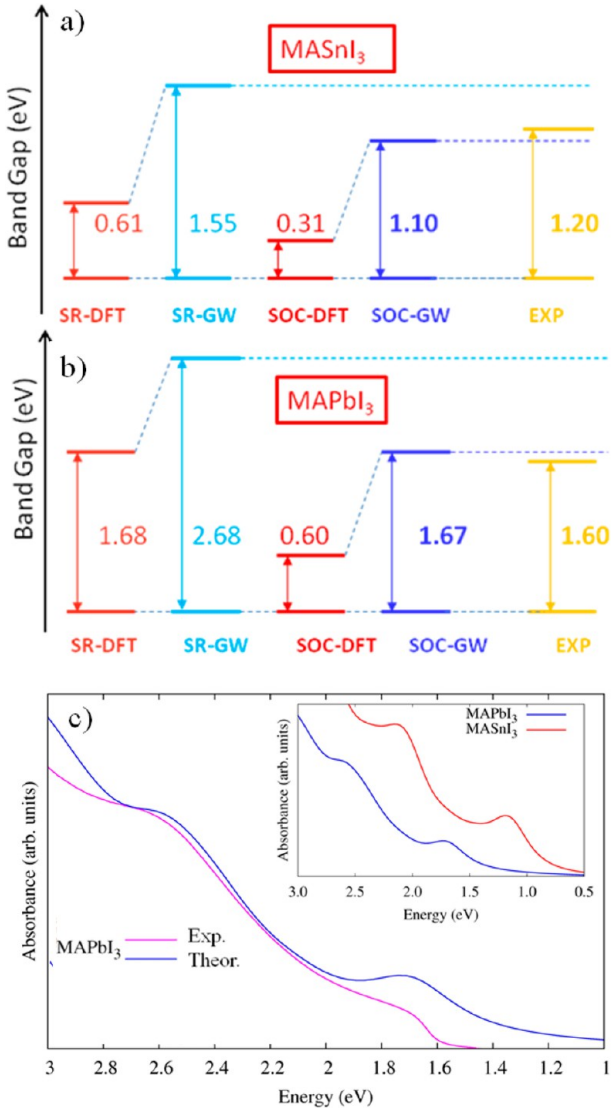

Figure 5. Calculated band gaps for $MASnI_3$ (a) and $MAPbI_3$ (b) perovskites. (c) Comparison between the experimental UV−vis spectrum of $MAPbI_3$ (red) and the SOC-GW calculated one (blue). Inset: Comparison between the SOC-GW calculated spectra of $MASnI_3$ (red) and $MAPbI_3$ (blue).

The investigated systems show a direct band gap at the Γ point of the Brilluoin zone. For $MAPbI_3$ and $MASnI_3$, the SR-DFT calculated band gaps are 1.68 and 0.61 eV, compared with experimental values of ∼1.6 and ∼1.2 eV, respectively. Thus, while for $MAPbI_3$ the band gap is (fortuitously) reproduced by SR-DFT, for $MASnI_3$ a 0.6 eV band gap underestimate is retrieved. Moving to SOC-DFT, the band gap values of both materials are strongly underestimated, by as much as 1 eV, although a qualitatively correct Pb → Sn band gap variation is calculated. SR-GW overestimates the $MAPbI_3$ band gap by ∼1 eV, while ∼0.3 eV band gap overestimate is found for $MASnI_3$, again leading to an unbalanced description. Rewardingly, SOC-GW delivers calculated band gaps in excellent agreement, within ±0.1 eV, with experimental values.

The SOC-GW optical absorption spectrum of $MAPbI_3$ and $MASnI_3$ was also simulated, albeit neglecting electron−hole interactions.[13] The results satisfactorily reproduce the experimental spectrum for $MAPbI_3$, Figure 5. Compared with $MAPbI_3$, the absorption spectrum of $MASnI_3$ shows a red shift (in line with the reduced band gap) and increased intensity, making this material attractive for photovoltaics applications.

2.3. Hole Transporters

The calculation of hole-transporter oxidation potentials is important for the fast and effective screening of new materials and for a description of sensitized metal-oxide/hole-transporter heterointerfaces. The most successful hole transporter in solid-state devices is Spiro-MeO-TAD, Figure 6, while record DSC efficiencies with liquid electrolytes have been obtained with Co(II)/Co(III) redox shuttles, see $[Co(bpy)_3]^{2+/3+}$ in Figure 6. In both cases, the hole-transporter oxidation potential stands at ∼5 eV vs vacuum.

The B3LYP-calculated oxidation potential for Spiro-MeO-TAD in ethanol was 4.27 eV,[29] sizably underestimating the experimental value. The negative of the HOMO value calculated by B3LYP (MPW1K) was 4.42 (5.36) eV. Although this data highlights the sizable dependence on the DFT choice in predicting the oxidation potentials of conjugated organic molecules, substituent trends within a given material are expected to be accurately reproduced. For a series of substituted cobalt complexes, instead, B3LYP quantitatively reproduced the absolute potentials within 0.1−0.2 eV, Table 2.[30]

2.4. TiO_2 Surfaces and Nanoparticles

TiO_2 is the established metal oxide in DSCs, mainly in the form of sintered nanoparticles of ∼20 nm size. The natural framework to describe TiO_2 surfaces is within periodic boundary conditions, in which an infinite and periodic solid can be effectively modeled. This choice translates in most cases in the use of nonhybrid DFT functionals, which are most common in codes using plane waves basis sets. For TiO_2, nonhybrid DFT provides a substantial band gap underestimate while hybrid DFT delivers an improved estimate compared with the experimental TiO_2 band gap value of 3.2 eV. Despite the band gap underestimate, nonhybrid DFT is widely used to obtain reasonably accurate geometrical structures efficiently. To take advantage of the typical quantum chemistry machinery (e.g., TDDFT with hybrid functional and continuum solvation models) in calculating the properties of dyes@TiO_2, we have over time developed a cluster approach to the description of TiO_2 based on the original concept of Persson and co-workers.[31] The calculated density of states (DOS) for a series of $(TiO_2)_n$ clusters of increasing dimensions gradually displayed quasi-continuous valence and conduction bands, with no apparent defect states in the band gap, and converged to stable energy values above ∼1 nm size (n = 38).[31] Furthermore, we verified that a $(TiO_2)_{82}$ cluster delivered a comparable DOS to that of a periodic $(TiO_2)_{32}$ slab, Figure 7a.[32] Most notably, the $(TiO_2)_{82}$ cluster also provided a CB edge energy of −3.76 eV vs vacuum, as estimated by TDDFT, almost coincident with the experimental value,[32] thus allowing us to investigate the alignment of energy levels in a series of dye@TiO_2 systems. We also extended the cluster approach to the study of the electronic structure and trap states in realistically large nanoparticles and nanorods, Figure 7b, although due to the large dimensions of these systems nonhybrid and semiempirical DFT was used.[33]

The cluster approach is a natural framework to investigate the interaction of one (or a few) dyes on the TiO_2 surface, but a periodic approach is to be preferred for the interaction of inherently periodic crystalline materials, for example, perovskites or other inorganic absorbers, on TiO_2.

dx.doi.org/10.1021/ar500089n | Acc. Chem. Res. 2014, 47, 3349−3360

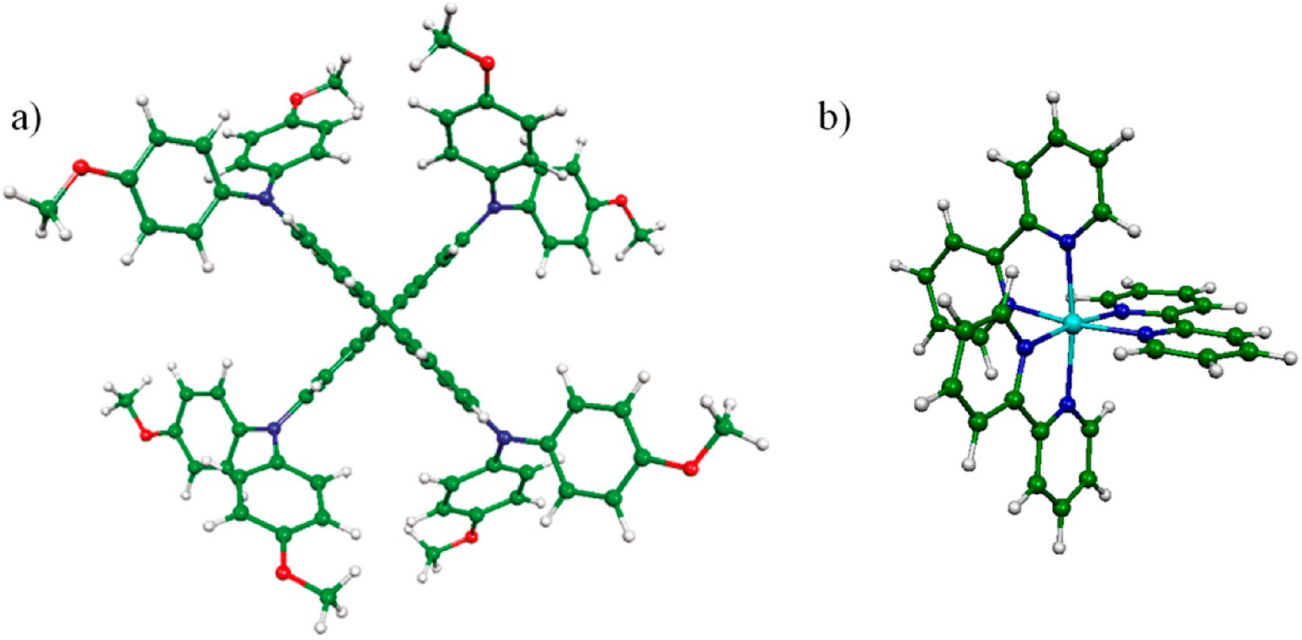

Figure 6. Optimized geometrical structures of (a) Spiro-MeO-TAD and (b) $[Co(bpy)_3]^{2+/3+}$.

Table 2. Oxidation Potential (ΔE_{OX}) for a Series of Cobalt Complexes Calculated by B3LYP/6-311G* in Acetonitrile

		ΔG_{OX}	
compound[a]	R	theor	expt
$[Co(R\text{-}bpy)_3]^{2+/3+}$	CH_3	4.87	4.87
	$C(CH_3)$	4.85	4.87
	H	5.06	5.00
	Cl	5.42	*b*
$[Co(R\text{-}phen)_3]^{2+/3+}$	H	5.15	5.06
	Cl	5.32	5.16
	NO_2	5.48	5.29
$[Co(py\text{-}pz)_2]^{2+/3+}$	H	5.42	5.40
$[Co(bpy\text{-}pz)_2]^{2+/3+}$	H	5.31	5.30
$[Co(R\text{-}tpy)_2]^{2+/3+}$	H	4.86	4.93
	Cl	5.10	5.07
	Cl-phen	4.87	4.91

[a]Bpy, phen, py, pz, and tpy stand, respectively, for bipyridine, phenanthroline, pyridine, pyrazole, and terpyridine. [b]Not available.

3. INTERFACES

The study of interfaces represents the most difficult task for hybrid/organic photovoltaics modeling, due to the inherent complexity of the investigated systems. Car−Parrinello molecular dynamics simulations can help in this challenging task, allowing us to sample the complex potential energy surface in search of local minima. Also, Car−Parrinello simulations allow us to study dynamic fluctuations in, for example, dye-sensitized metal oxide and the surrounding solvent.[34] Here we briefly describe three relevant interfaces using selected examples, that is, dye/metal oxide, dye/metal oxide/hole transporter, and perovskite/metal oxide.

3.1. Ruthenium Dye-Sensitized TiO_2

In DSCs, the dye/metal-oxide interactions are mediated by the dye adsorption mode onto the oxide surface, occurring via suitable anchoring groups. The dye anchoring group should coincide with, or be very close (conjugated) to, the dye acceptor unit, where the photoexcited electrons are spatially confined. This promotes electronic coupling between the donor

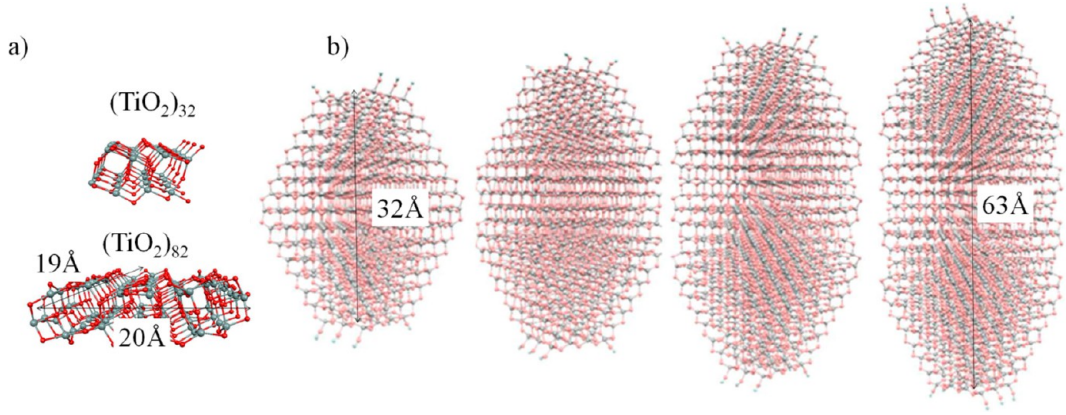

Figure 7. (a) Structure of a $(TiO_2)_{32}$ periodic slab (top) and of a $(TiO_2)_{82}$ cluster (bottom). (b) $(TiO_2)_n$ nanocrystals and nanorods of increasing dimension. Structures in parts a and b are drawn on different scales.

dx.doi.org/10.1021/ar500089n | *Acc. Chem. Res.* 2014, 47, 3349−3360

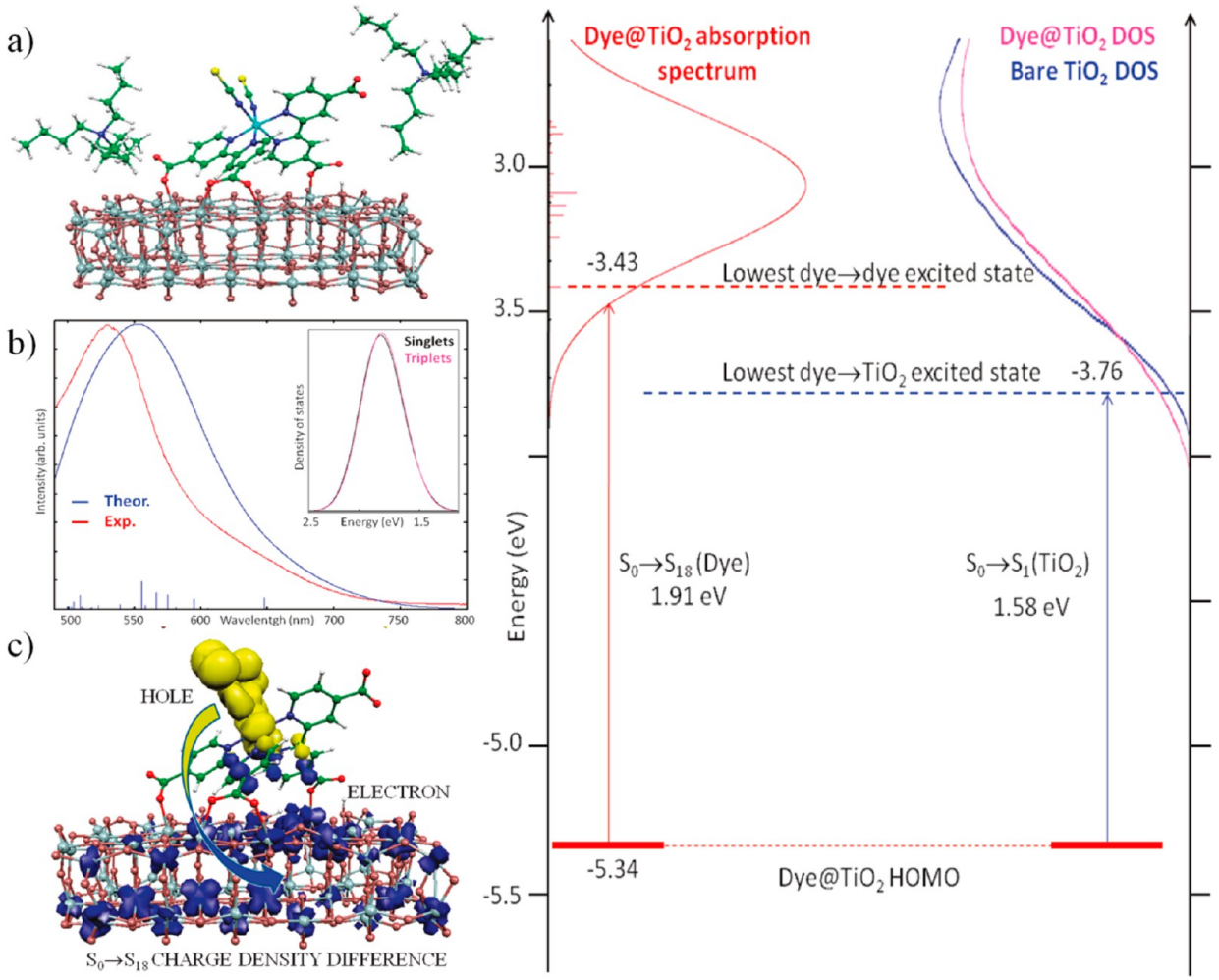

Figure 8. (left) (a) Optimized adsorption geometry of the N719 dye (notice the two TBA counterions) on $(TiO_2)_{82}$. (b) Comparison between the experimental (red) and TDDFT-calculated (blue) optical absorption spectrum for N719@$(TiO_2)_{82}$ with no *tert*-butylammonium counterions. (c) Charge density difference between the ground state (S_0) and the S_{18} excited state. A blue color signifies a charge density increase and yellow a decrease. (right) Alignment of energy levels for N719@$(TiO_2)_{82}$.

levels of the excited dye and the delocalized metal-oxide acceptor levels, assisting charge injection. The orientation and packing of dyes on the metal-oxide surface may also affect parasitic recombination reactions. Finally, the sensitizer's anchoring group should provide stable grafting of the dye onto the semiconductor surface, leading to long-term device stability. It is thus fundamental to disclose the adsorbing mode shown by the most commonly employed sensitizers. This is however a formidable task, since even considering a single carboxylic anchor there are various adsorption modes available within a relatively narrow energy range,[35] whose relative stability may be influenced by the environment. Furthermore, different DFT methods and different TiO_2 models deliver different relative stabilities.[35] The situation is even more complex in ruthenium dyes, for example, N3/N719, characterized by up to four carboxylic groups. In this case, one should calculate all the possible adsorption modes[36] or alternatively employ Car−Parrinello dynamics to obtain a global, rather than detailed, picture of the interface. Based on Car−Parrinello simulations of the N719 dye@$(TiO_2)_{38}$, Supporting Information, we found that the N719 dye, with or without *tert*-butylammonium counterions, preferentially adsorbs on TiO_2 exploiting three carboxylic groups, Figure 8a.

For N719@$(TiO_2)_{82}$, we thus calculated the lowest 50 singlet−singlet excited states by B3LYP/TDDFT in solution, allowing us to simulate the optical absorption spectrum up to ∼2.5 eV, Figure 8b. The agreement between the calculated and experimental spectra is excellent, in terms of both spectral shape and absorption maxima (552 nm/2.25 eV compared with 531 nm/2.34 eV). The charge density difference of the lowest optically active state ($S_0 \rightarrow S_{18}$, at 649 nm/1.91 eV), Figure 8c, is illustrative of the strong dye/TiO_2 unoccupied states admixture. Light absorption thus leads to a photoexcited electron partly delocalized on TiO_2. Notably, this almost "direct" injection mechanism, mediated by the dye excited states, is possibly signaled by the shoulder in the experimental spectrum seen at the calculated $S_0 \rightarrow S_{18}$ energy, Figure 8b.

We now turn to the alignment of energy levels in N719@$(TiO_2)_{82}$, for which we need to fix a relative energy scale. This is conveniently realized by taking as a reference the energy of the dye HOMO, which was shown to represent a good approximation to the dye oxidation potential in solution.[20] We can thus approximately locate the lowest TiO_2-based excited state simply by adding the energy of the TDDFT $S_0 \rightarrow S_1$ transition (1.58 eV) to the HOMO energy. By superimposing the combined systems' absorption spectrum

dx.doi.org/10.1021/ar500089n | *Acc. Chem. Res.* 2014, 47, 3349−3360

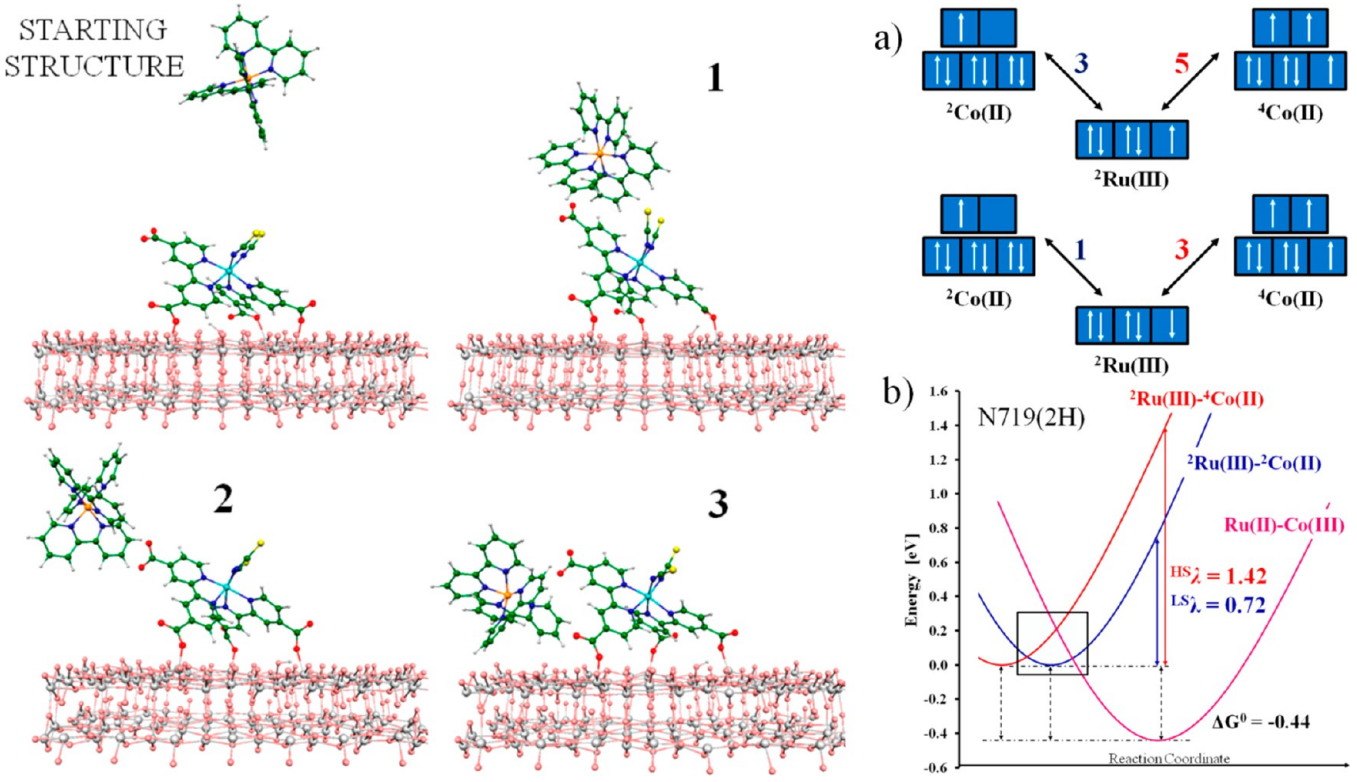

Figure 9. (left) Sequence of representative geometrical structures for the N719@TiO_2/$[Co(bpy)_3]^{3+}$ system extracted from the CPMD simulation. (right) (a) Possible coupling patterns between ^{2}Co(II), ^{4}Co(II), and ^{2}Ru(III). (b) High-spin (HS) and low-spin (LS) reaction profiles for N719 regeneration by $[Co(bpy)_3]^{2+}$.

to the energy scale relative to the dye HOMO, Figure 8, we can accordingly calculate the lowest dye-based excited state ~0.3 eV above the lowest TiO_2 state, this energy representing the lowest driving force for electron injection. Notably, the absorption spectrum of the combined system very well matches with the density of unoccupied states in both sensitized and unsensitized TiO_2. This is an essential requisite, along with the spatial excited state coupling, ensured by the nature of the excited states, to have very efficient ultrafast electron injection,[25] as is effectively observed in this system.

3.2. Dye-Sensitized TiO_2/Cobalt Hole-Transporter Interface

As mentioned above, the highest DSC efficiency was obtained for devices employing a Co(II)/Co(III) hole transporter together with a porphyrin dye.[2] Surprisingly, the prototypical high-efficiency N719 ruthenium dye delivered dramatically low photovoltaic efficiency, ~2%, with Co(II)/Co(III) hole transporters.[30] Considering that N719 carries four carboxylic/carboxylate groups, the formation of ion-pairs between the negatively charged, TiO_2-adsorbed N719 dye and Co(III) species could limit the DSC efficiency. To gain insight into the possible interactions occurring at the triple dye/metal-oxide/hole-transporter interface, we carried out Car−Parrinello simulations of N719 adsorbed onto a periodic TiO_2 surface slab in the presence of the oxidized $[Co(bpy)_3]^{3+}$ species, Figure 9. This model is obviously limited, lacking solvent molecules and counterions though it is useful to qualitatively explore the interface potential energy landscape.

From the Car−Parrinello simulation, Supporting Information, we extracted three representative structures, Figure 9, which have been optimized in solution. For the monoprotonated N719, a sizable $[Co(bpy)_3]^{3+}$ binding energy was calculated, ranging from 0.60 to 0.16 eV depending on the number (0 to 3) of $[Co(bpy)_3]^{3+}$ counterions. Notably, the presence of interacting N719/$[Co(bpy)_3]^{3+}$ species was also proven experimentally,[30] confirming their possible role in decreasing the efficiency of N719-sensitized solar cells.

Another interesting and largely unexplored aspect of Co(II)/Co(III) hole transporters concerns the oxidized dye regeneration mechanism. The d^7 Co(II) complexes are characterized by almost degenerate low-spin (^{2}Co(II)) and high-spin (^{4}Co(II)) states. Co(III) complexes are instead closed-shell d^6 singlets. Since dye regeneration consists of electron transfer from the ^{2,4}Co(II) complexes to the oxidized dye, giving the Co(III) complex, both high-spin and low-spin Co(II) could, in principle, contribute to the dye regeneration, with possibly different kinetics. We thus simulated the possible Co(II)−Ru(III) couples, formed after injection of one electron from the dye excited state to TiO_2, Figure 9a. We then analyzed the dye regeneration within Marcus theory framework, by calculating the complexes' reorganization energies and driving forces for both the high-spin and low-spin pathways. The results, Figure 9b, show that the low-spin pathway is favored by the lower reorganization energy. Thus, if a high-spin Co(II) complex is the starting state, as is the case of $[Co(bpy)_3]^{2+}$,[30] a spin-crossover barrier could slow the dye regeneration process, while starting low-spin species (such as $[Co(tpy)_2]^{2+}$) could exhibit faster regeneration kinetics.

3.2. Perovskite-Sensitized TiO_2

As a last example, we illustrate recent results obtained from the simulation of the $MAPbI_3$ perovskite/TiO_2 interface.[37] Our model system is made by a 3 × 5 × 3 pseudocubic perovskite slab, Figure 10a. The optimized slab has a SOC-PBE calculated

dx.doi.org/10.1021/ar500089n | Acc. Chem. Res. 2014, 47, 3349−3360

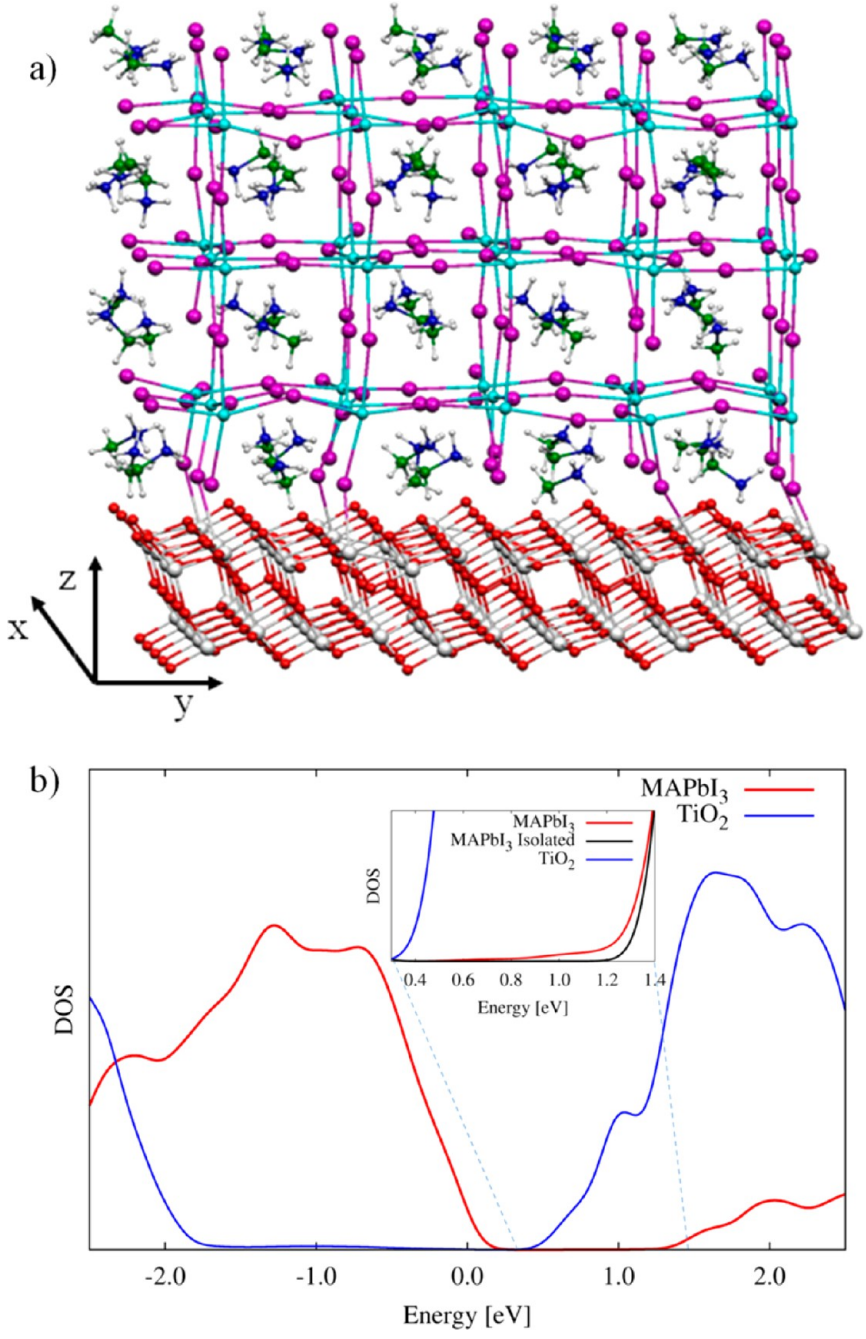

Figure 10. (a) Optimized structure of the simulated TiO_2/$MAPbI_3$ interface along with reference axes. (b) Calculated DOS including spin−orbit coupling for the TiO_2/$MAPbI_3$ interface, decomposed into the contributions of $MAPbI_3$ (red) and TiO_2 (blue). The inset shows the bottom of the interacting perovskite DOS, compared with the noninteracting DOS at the same geometry.

band gap of 1.50 eV, higher than the calculated bulk value of 0.60 eV, due to the confined slab. GW calculations are impractical for such a large system, so we proceeded by DFT. The perovskite model was "deposited" onto a 5 × 3 × 2 (101) TiO_2 anatase slab, Figure 10a. The experimental TiO_2 cell parameters were employed to build a periodic supercell in the *x* and *y* directions, with a lattice mismatch of only +0.75 and −1.85% along the *x* and *y* directions in the perovskite. The PBE-optimized geometries, Figure 10a, show the binding of perovskite iodine atoms to under-coordinated surface Ti(IV), along with the formation of several hydrogen bonds from the MA cations to surface oxygen atoms.

The SOC-PBE calculated DOS for the TiO_2/$MAPbI_3$ interface, Figure 10b, shows the perovskite CB to lie quite above the TiO_2 CB, in line with previous DFT results for the noninteracting fragments[12] and with experimental data.[3] Notice, however, that the employed DFT method is prone to underestimate the position of the TiO_2 CB energy and band gap, so the calculated TiO_2/$MAPbI_3$ CB offset (ca. 0.8 eV) is expected to be overestimated. The two materials are only weakly interacting, as seen by the little hybridization between perovskite Pb p states, maximally contributing to the CB, and Ti d orbitals constituting the TiO_2 CB. The hybridization can be visualized by comparing the CB bottom for the interacting TiO_2/$MAPbI_3$ system and for the isolated $MAPbI_3$ cut from the

dx.doi.org/10.1021/ar500089n | *Acc. Chem. Res.* 2014, 47, 3349−3360

optimized interface, inset of Figure 10b. This indicates a weak interfacial electronic coupling, quite opposite to the situation found in conventional dye-sensitized interfaces, suggesting a potentially different mechanism of charge generation.[37]

4. CONCLUSIONS

Computational modeling in hybrid/organic photovoltaics has been extremely successful to assist the design and screening of new materials and to provide hitherto inaccessible information related to the functioning of the crucial devices hetero-interfaces. DFT/TDDFT methods had a tremendous impact in the field, due to the excellent trade-off between accuracy and computational burden. The DSC field is reaching a mature stage, as are the related modeling strategies. The simulation of the electronic and optical properties of isolated dyes is nowadays a routine task and the study of dye/sensitized interfaces is becoming increasingly popular. Inclusion of SOC into DFT/TDDFT has further broadened the scope of these simulations. The limitations of DFT/TDDFT for the description of dye/sensitized interfaces and hole transporters mainly rest on the unbalanced description of systems characterized by a high degree of CT and of metal-oxide semiconductors. While future research on new DFT/TDDFT methods will likely encompass these problems, the use of GW methods appears to solve some of these issues but at the expenses of a larger computational overhead.

The recent "perovskite storm" has cast new problems on the playground. Again DFT represents the "first aid" method to approach this class of materials and the related interfaces, with SOC effects playing a major role. Efficient SOC-GW implementations allow us to correctly reproduce the materials electronic properties at a reasonable computational cost, but the relevant perovskite/TiO_2 or Al_2O_3 interfaces are still too big for a GW approach. Understanding exciton formation and dissociation and carrier recombination is nowadays the cutting-edge research in perovskite solar cells. I expect an integrated modeling strategy, based on a combination of different codes and techniques, to play a major role in further advancing the perovskite solar cells technology.

■ ASSOCIATED CONTENT

Supporting Information

Movies of Car−Parrinello simulations. This material is available free of charge via the Internet at http://pubs.acs.org.

■ AUTHOR INFORMATION

Corresponding Author

*E-mail: filippo@thch.unipg.it.

Funding

The author thanks FP7-ENERGY-2010 Project 261920 "ESCORT" for financial support.

Notes

The authors declare no competing financial interest.

Biography

Filippo De Angelis is senior research scientist and deputy director at the CNR Institute of Molecular Sciences and Technology in Perugia, Italy. He is the founder and coleader of the Computational Laboratory for Hybrid/Organic Photovoltaics (CLHYO). He earned a B.S. in Chemistry 1996 and a Ph.D. in Theoretical Inorganic Chemistry in 1999, both from the University of Perugia, Italy. He is an expert in the development and application of quantum chemical methods to study the structural, electronic, and optical properties of complex systems including transition metals. His main research interests are in the field of hybrid/organic photovoltaics. He is the 2007 recipient of the Raffaello Nasini Gold Medal of the Inorganic Chemistry Division of the Italian Chemical Society.

■ REFERENCES

(1) O'Regan, B.; Grätzel, M. A Low-Cost, High-Efficiency Solar Cell Based on Dye-Sensitized Colloidal TiO_2 Films. *Nature* **1991**, *353*, 737−740.

(2) Mathew, S.; Yella, A.; Gao, P.; Humphry-Baker, R.; Curchod, B. F. E.; Ashari-Astani, N.; Tavernelli, I.; Rothlisberger, U.; Nazeeruddin, M. K.; Grätzel, M. Dye-Sensitized Solar Cells with 13% Efficiency Achieved through the Molecular Engineering of Porphyrin Sensitizers. *Nat. Chem.* **2014**, *6*, 242−247.

(3) Kim, H.-S.; Lee, C.-R.; Im, J.-H.; Lee, K.-B.; Moehl, T.; Marchioro, A.; Moon, S.-J.; Humphry-Baker, R.; Yum, J.-H.; Moser, J. E. Lead Iodide Perovskite Sensitized All-Solid-State Submicron Thin Film Mesoscopic Solar Cell with Efficiency Exceeding 9%. *Sci. Rep.* **2012**, *2*, No. 591.

(4) Burschka, J.; Pellet, N.; Moon, S.-M.; Humphry-Baker, R.; Gao, P.; Nazeeruddin, M. K.; Grätzel, M. Sequential Deposition As a Route to High-Performance Perovskite-Sensitized Solar Cells. *Nature* **2013**, *499*, 316−319.

(5) Lee, M. M.; Teuscher, J.; Miyasaka, T.; Murakami, T. N.; Snaith, H. J. Efficient Hybrid Solar Cells Based on Meso-Superstructured Organometal Halide Perovskites. *Science* **2012**, *338*, 643−647.

(6) Liu, M.; Johnston, M. B.; Snaith, H. J. Efficient Planar Heterojunction Perovskite Solar Cells by Vapour Deposition. *Nature* **2013**, *501*, 395−398.

(7) Labat, F.; Le Bahers, T.; Ciofini, I.; Adamo, C. First-Principles Modeling of Dye-Sensitized Solar Cells: Challenges and Perspectives. *Acc. Chem. Res.* **2012**, *45*, 1268−1277.

(8) Prezhdo, O. V.; Duncant, W. R.; Prezhdo, V. V. Dynamics of the Photoexcited Electron at the Chromophore−Semiconductor Interface. *Acc. Chem. Res.* **2008**, *41*, 339−348.

(9) Fantacci, S.; De Angelis, F.; Fantacci, S.; De Angelis, F. A Computational Approach to the Electronic and Optical Properties of Ru(II) and Ir(III) Polypyridyl Complexes: Applications to DSC, OLED and NLO. *Coord. Chem. Rev.* **2011**, *255*, 2704−2726.

(10) Martsinovich, N.; Troisi, A. Theoretical Studies of Dye-Sensitised Solar Cells: From Electronic Structure to Elementary Processes. *Energy Environ. Sci.* **2011**, *4*, 4473−4495.

(11) Mosconi, E.; Amat, A.; Nazeeruddin, M. K.; Grätzel, M.; De Angelis, F. First-Principles Modeling of Mixed Halide Organometal Perovskites for Photovoltaic Applications. *J. Phys. Chem. C* **2013**, *117*, 13902−13913.

(12) Even, J.; Pedesseau, L.; Jancu, J.-M.; Katan, C. Importance of Spin−Orbit Coupling in Hybrid Organic/Inorganic Perovskites for Photovoltaic Applications. *J. Phys. Chem. Lett.* **2013**, *4*, 2999−3005.

(13) Umari, P.; Mosconi, E.; De Angelis, F. Relativistic GW Calculations on $CH_3NH_3PbI_3$ and $CH_3NH_3SnI_3$ Perovskites for Solar Cell Applications. *Sci. Rep.* **2014**, *4*, No. 4467.

(14) Car, R.; Parrinello, M. Unified Approach for Molecular Dynamics and Density-Functional Theory. *Phys. Rev. Lett.* **1985**, *55*, 2471−2474.

(15) Rego, L. G. C.; Batista, V. S. Quantum Dynamics Simulations of Interfacial Electron Transfer in Sensitized TiO_2 Semiconductors. *J. Am. Chem. Soc.* **2003**, *125*, 7989−7997.

(16) Nazeeruddin, M. K.; De Angelis, F.; Fantacci, S.; Selloni, A.; Viscardi, G.; Liska, P.; Ito, S.; Takeru, B.; Grätzel, M. Combined Experimental and DFT-TDDFT Computational Study of Photoelectrochemical Cell Ruthenium Sensitizers. *J. Am. Chem. Soc.* **2005**, *127*, 16835−16847.

(17) Kinoshita, T.; Dy, J. T.; Uchida, S.; Kubo, T.; Segawa, H. Wideband Dye-Sensitized Solar Cells Employing a Phosphine-Coordinated Ruthenium Sensitizer. *Nat. Photonics* **2013**, *7*, 535−539.

(18) Fantacci, S.; De Angelis, F.; Selloni, A. Absorption Spectrum and Solvatochromism of the [Ru(4,4′-COOH-2,2′-bpy)$_2$(NCS)$_2$] Molecular Dye by Time Dependent Density Functional Theory. *J. Am. Chem. Soc.* **2003**, *125*, 4381−4387.
(19) De Angelis, F.; Fantacci, S.; Selloni, A.; Nazeeruddin, M. K. Time Dependent Density Functional Theory Study of the Absorption Spectrum of the [Ru(4,4′-COO–2,2′-bpy)$_2$(X)$_2$]$^{4-}$ (X = NCS, Cl) Dyes in Water Solution. *Chem. Phys. Lett.* **2005**, *415*, 115−120.
(20) De Angelis, F.; Fantacci, S.; Selloni, A. Alignment of the Dye's Molecular Levels with the TiO_2 Band Edges in Dye-Sensitized Solar Cells: A DFT-TDDFT Study. *Nanotechnology* **2008**, *19*, No. 424002.
(21) Fantacci, S.; Ronca, E.; De Angelis, F. Impact of Spin−Orbit Coupling on Photocurrent Generation in Ruthenium Dye-Sensitized Solar Cells. *J. Phys. Chem. Lett.* **2014**, *5*, 375−380.
(22) Wang, F.; Ziegler, T. A. Simplified Relativistic Time-Dependent Density-Functional Theory Formalism for the Calculations of Excitation Energies Including Spin-Orbit Coupling Effect. *J. Chem. Phys.* **2005**, *123*, No. 154102.
(23) Pastore, M.; Mosconi, E.; De Angelis, F.; Graetzel, M. A Computational Investigation of Organic Dyes for Dye-Sensitized Solar Cells: Benchmark, Strategies, and Open Issues. *J. Phys. Chem. C* **2010**, *114*, 7205−7212.
(24) Pastore, M.; Fantacci, S.; De Angelis, F. Ab Initio Determination of Ground and Excited State Oxidation Potentials of Organic Chromophores for Dye-Sensitized Solar Cells. *J. Phys. Chem. C* **2010**, *114*, 22742−22750.
(25) Pastore, M.; Fantacci, S.; De Angelis, F. Modeling Excited States and Alignment of Energy Levels in Dye-Sensitized Solar Cells: Successes, Failures, and Challenges. *J. Phys. Chem. C* **2013**, *117*, 3685−3700.
(26) Umari, P.; Giacomazzi, L.; De Angelis, F.; Pastore, M.; Baroni, S. Energy-Level Alignment in Organic Dye-Sensitized $TiO_2$from GW Calculations. *J. Chem. Phys.* **2013**, *139*, No. 014709.
(27) Castelli, I. E.; Olsen, T.; Datta, S.; Landis, D. D.; Dahl, S.; Thygesen, K. S.; Jacobsen, K. W. Computational Screening of Perovskite Metal Oxides for Optimal Solar Light Capture. *Energy Environ. Sci.* **2012**, *5*, 5814−5819.
(28) Sakuma, R.; Friedrich, C.; Miyake, T.; Blügel, S.; Aryasetiawan, F. GW Calculations Including Spin-Orbit Coupling: Application to Hg Chalcogenides. *Phys. Rev. B* **2011**, *84*, No. 085144.
(29) Fantacci, S.; De Angelis, F.; Nazeeruddin, M. K.; Graetzel, M. Electronic and Optical Properties of the Spiro-MeOTAD Hole Conductor in Its Neutral and Oxidized Forms: A DFT/TDDFT Investigation. *J. Phys. Chem. C* **2011**, *115*, 23126−23133.
(30) Mosconi, E.; Yum, J. H.; Kessler, F.; Gomez-Garcia, C. J.; Zuccaccia, C.; Cinti, A.; Nazeeruddin, M. K.; Graetzel, M.; De Angelis, F. Cobalt Electrolyte/Dye Interactions in Dye-Sensitized Solar Cells: A combined Computational and Experimental Study. *J. Am. Chem. Soc.* **2012**, *134*, 19438−19453.
(31) Lundqvist, M. J.; Nilsing, M.; Persson, P.; Lunell, S. DFT Study of Bare and Dye-Sensitized TiO_2 Clusters and Nanocrystals. *Int. J. Quantum Chem.* **2006**, *106*, 3214−3234.
(32) De Angelis, F.; Fantacci, S.; Mosconi, E.; Nazeeruddin, M. K.; Grätzel, M. Absorption Spectra and Excited State Energy Levels of the N719 Dye on TiO_2 in Dye-Sensitized Solar Cell Models. *J. Phys. Chem. C* **2011**, *115*, 8825−8831.
(33) Nunzi, F.; Mosconi, E.; Storchi, L.; Ronca, E.; Selloni, A.; Grätzel, M.; De Angelis, F. Inherent Electronic Trap States in TiO_2 Nanocrystals: Effect of Saturation and Sintering. *Energy Environ. Sci.* **2013**, *6*, 1221−1229.
(34) De Angelis, F.; Fantacci, S.; Gebauer, R. Simulating Dye-Sensitized TiO_2 Heterointerfaces in Explicit Solvent: Absorption Spectra, Energy Levels, and Dye Desorption. *J. Phys. Chem. Lett.* **2011**, *2*, 813−817.
(35) Anselmi, C.; Mosconi, E.; Pastore, M.; Ronca, E.; De Angelis, F. Adsorption of Organic Dyes on TiO_2 Surfaces in Dye-Sensitized Solar Cells: Interplay of Theory and Experiment. *Phys. Chem. Chem. Phys.* **2012**, *14*, 15963−15974.
(36) Martsinovich, N.; Ambrosio, F.; Troisi, A. Adsorption and Electron Injection of the N3 Metal−Organic Dye on the TiO2 Rutile (110) Surface. *Phys. Chem. Chem. Phys.* **2012**, *14*, 16668−16676.
(37) Roiati, V.; Mosconi, E.; Listorti, A.; Colella, S.; Gigli, G.; De Angelis, F. Stark Effect in Perovskite/TiO_2 Solar Cells: Evidence of Local Interfacial Order. *Nano Lett.* **2014**, *14*, 2168−2174.